Five-Year Climatology of Midtroposphere Dry Air Layers in Warm Tropical Ocean Regions as Viewed by AIRS/*Aqua*

SEAN P. F. CASEY, ANDREW E. DESSLER, AND COURTNEY SCHUMACHER

Department of Atmospheric Sciences, Texas A&M University, College Station, Texas

(Manuscript received 12 August 2008, in final form 16 February 2009)

ABSTRACT

Many studies have commented on the presence of midtroposphere dry air layers in normally moist areas of the warm-pool region in the tropical western Pacific Ocean. In this study, 5 yr of relative humidity (RH) observations from the Atmospheric Infrared Sounder (AIRS) instrument aboard the *Aqua* satellite are analyzed to identify areas of anomalously dry air between 600 and 400 hPa over deep convective regions of the tropical oceans. A dry air layer is defined when midlevel RH is <20%, accounting for the lowest 10% of RH observations. Dry air layers appear to be more frequent over the Indian and Pacific Oceans than over the Atlantic Ocean. Large seasonal differences in the locations of dry air layers are apparent in each ocean basin. Large variations are also noted across the Pacific, suggesting limits on the applicability of case-study trends and observations of dry air layers to the Pacific as a whole. Back trajectories are then calculated for each observed parcel. The origin, or location of dehydration, is identified as the point along each trajectory at which the RH of the parcel is ≥100%. An analysis of the time between dehydration and dry air observation by AIRS suggests that dry air layers in June–August tend to last 1–2 days longer than those observed in other seasons. Although more dry air layers are observed to come from each hemisphere in its respective winter, most sources of dry air layers are subtropical and contribute anomalously dry air year-round. Other meteorological features are noted in the back trajectories, such as the eastward/westward wind transition from the subtropics to the tropics and the effects of the Indian monsoon on dry air distribution paths.

1. Introduction

Johnson et al. (1999) has become a landmark paper in tropical meteorology, providing clear evidence and analysis of a trimodal distribution of tropical convective clouds: *shallow convective* clouds with cloud-top heights near 2 km above the surface, *cumulus congestus* clouds with tops near 5 km, and *cumulonimbus* clouds capped by the tropopause. However, although the capping mechanisms behind shallow and deep convection are well understood (Simpson 1992), Johnson et al. (1999) lacked the data to account for the limiting factors of midlevel congestus cloud-top heights.

The explanation of congestus cloud-top heights has recently turned to anomalously warm and dry midtropospheric conditions noted by Johnson et al. (1996). Dry air from aloft in higher latitudes enters the tropics and subsides in long filaments hundreds of kilometers in width. Yoneyama and Parsons (1999) related these layers to Rossby wave breaking and tracked the source back to midlatitude baroclinic waves. Whereas the lower and middle atmosphere (below ~8 km) recovered to moist conditions within a week (Parsons et al. 2000), the upper atmosphere (above 8 km) remained anomalously dry for 10–20 days.

Redelsperger et al. (2002) analyzed the effects of a dry layer observed during the Tropical Ocean and Global Atmosphere Coupled Ocean–Atmosphere Response Experiment (TOGA COARE) using a cloud-resolving model. Following the layer's entrance into the study area, moisture in the lower troposphere and midtroposphere recovered as a result of convection penetrating into the dry air mass. The most common mode of convection was congestus clouds of ~4–6 km in height, and the authors suggested that the dry air layer decreased parcel buoyancy, controlling the cloud top.

Jensen and Del Genio (2006) studied soundings from the Atmospheric Radiation Measurement Program research facility at Nauru Island and analyzed them with a

Corresponding author address: Sean P. F. Casey, Department of Atmospheric Sciences, Texas A&M University, 3150 TAMU, College Station, TX 77840.
E-mail: scasey@ariel.met.tamu.edu

DOI: 10.1175/2009JAMC2099.1

parcel model. This study also showed that a drying of the midtroposphere was more of a factor in limiting congestus cloud-top height than the 0°C stable layer [described in Johnson et al. (1996)]. Zuidema et al. (2006) focused on data from the R/V *Ronald H. Brown* obtained during the 2002 East Pacific Investigation of Climate (EPIC) experiment. This study showed that even outside the western Pacific Ocean warm pool, dry air layers were associated with high populations of cumulus congestus clouds.

Midtropospheric dry layers also have implications in global-warming theory. Pierrehumbert (1995) noted the importance of dry ''radiator fins,'' maintained by subsidence, in regulating tropical temperature and preventing a ''runaway greenhouse effect.'' Spencer and Braswell (1997) compared new microwave humidity sounder data with general circulation model (GCM) analyses, discovering that the GCM humidity values in the free troposphere were overestimated in these dry regions. Zhang et al. (2003) noted the overall bimodality of tropical free tropospheric humidity and that GCMs did not accurately represent the drier mode.

The previous discussion highlights the importance of tropical midlevel dry air, but no global climatological description (''climatology'') of the occurrence or sources of midlevel dry air layers exists. Other studies (Waugh and Polvani 2000; Waugh and Funatsu 2003; Ryoo et al. 2008) provide climatologies on tropical upper-troposphere dry air intrusions originating in the stratosphere, but their analyses do not extend to the 0°C melting level at which congestus tops commonly occur (Johnson et al. 1999). Case studies have noted anomalously dry midtropospheric layers in the Indian Ocean (Zachariasse et al. 2001), but having a clearer picture of this global distribution would not only enhance understanding of the limiting factors of congestus clouds but would also have greater implications for global-warming theory. In this paper, we analyze the location, frequency, and source regions of dry air layers over the tropical oceans with an eye toward answering the following questions: What is the applicability of the previous Pacific Ocean regional case studies to the rest of the basin? Can these be applied to the Indian and Atlantic Oceans as well, or are there clear differences among the three basins? How does the distribution of such layers vary by season? Where do these dry air layers originate, and how does this distribution vary seasonally?

This paper aims to answer these questions using 5 yr of satellite-based relative humidity measurements. Section 2 describes the data source and method for identification of midlevel dry air layers. Section 3 analyzes the distribution observed in each ocean basin, along with seasonal separation. Section 4 uses a back-trajectory model to determine where parcels within these dry air layers were last saturated. Section 5 returns to the preceding questions and discusses future areas of research.

2. Humidity observations

To identify dry air layers, water vapor mixing ratio measurements were taken from the Atmospheric Infrared Sounder (AIRS) instrument onboard the *Aqua* satellite. AIRS retrievals have an effective resolution of ~50 km in the horizontal direction and 2 km in the vertical direction, with an accuracy of within ~10% for any individual measurement (Fetzer et al. 2005). Five years of near-continuous version-5, level-2 data between September of 2002 and August of 2007 were used. The potential effects of such dry air anomalies would be most prevalent in deep convective regions over the warm tropical oceans [where the trimodal distribution identified by Johnson et al. (1999) is prevalent]. Therefore, we limit our analysis to oceanic areas where the long-term (1968–96) monthly mean outgoing longwave radiation (OLR), as measured by National Oceanic and Atmospheric Administration (NOAA) polar-orbiting satellites and obtained from the National Centers for Environmental Prediction (NCEP; Liebmann and Smith 1996), was less than 240 W m^{-2}. This threshold reduces the study area to only those areas in which deep convection is most prevalent (thus lowering the long-term mean OLR) and where the upper atmosphere would be expected to be the most humid given the prevalence of deep convective processes.

Figure 1 shows the frequency of occurrence at each pressure level for each level-2 relative humidity measurement with respect to liquid for temperature $T >$ 273 K and ice otherwise. In this and all following figures, observations at a given location and month were used only if the monthly mean OLR in that location and month was less than 240 W m^{-2}. The total values at each pressure level add up to 1. This figure shows that, although the air above the tropical oceans is normally very moist, there are occurrences of anomalously dry air. Plotted over this are the mean relative humidty (RH) profiles from the AIRS measurements (dashed) and from TOGA COARE (solid; Ciesielski et al. 2003). These profiles suggest that, when taken over the full warm tropical maritime region, mean RH values are lower between 600 and 400 hPa than during TOGA COARE, which was limited to the warm pool of the western Pacific.

Using relative humidity data over the eastern Pacific during the EPIC campaign, Zuidema et al. (2006) defined midlevel dry air layers as those instances in which the RH between 400 and 600 hPa was less than 40%.

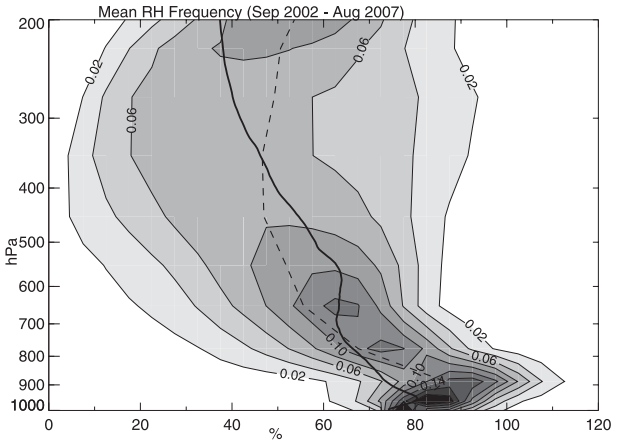

FIG. 1. Relative frequency of mean RH values over warm (mean monthly OLR < 240 W m^{-2}) oceanic regions, as a function of height. The RH values are grouped into 5% bins, and the vertical bin is based on pressure levels given in version-5 AIRS data. The sum of all values at each pressure level adds to 1. The vertical dashed line marks the mean profile, and the solid line denotes the mean TOGA COARE RH profile (Ciesielski et al. 2003).

Although 40% is a low value for midlevel RH in Fig. 1, it is by no means anomalous. Brown and Zhang (1997) noted a range of 60% in midtroposphere RH during TOGA COARE between rainy and drought periods, with frequent observations at or below 20% RH during a drought period when lower cloud-top heights were more frequent. To analyze the driest RH sources while still using enough data to be statistically significant, we chose to analyze the lowest 10% of the data. Cumulative distribution function (CDF) analysis (not shown) suggests that this 10% threshold is near RH values of 20% in the Indian and Pacific Oceans and 25% in the Atlantic Ocean. To use the same threshold globally and given the greater area of the Indian and Pacific Oceans relative to that of the Atlantic, we decided to define dry air layers for this study as those areas in which RH at these altitudes was less than 20%, using the same pressure bounds (400 and 600 hPa) used by Zuidema et al. (2006). Although this threshold is somewhat arbitrary, changes to the threshold (between 15% and 25%) suggested little change in the relative dry air layer distribution between ocean bodies. This threshold also coincides with the most frequent RH observations during dry periods noted by Brown and Zhang (1997).

3. Dry air distributions

Figure 2 shows the frequency of midlevel dry air layers over the tropical oceans, graphed into 2.5° grid resolution. The frequency is the number of dry air observations in a bin divided by the total number of AIRS observations within that bin times 100. The thick solid line marks the boundary of areas where the long-term mean OLR is less than 240 W m^{-2} for at least one calendar month. Figures 3–5 will focus on individual ocean basins. A similar color bar and contour system is used on each figure so as to make interfigure comparisons easier.

a. Atlantic Ocean

Figure 2 shows that over the Atlantic Ocean dry midlevel air is most frequently observed (i.e., ~25% of the time) around 12°N between 45° and 25°W. Adjustment of the upper RH threshold between 15% and 25% (not shown) revealed a change in the maximum frequency observation of less than 5%. Otherwise, the frequency of dry air observations is low, around 5% over much of the Atlantic.

Figure 3 separates the total dry air distribution over the Atlantic by season. The maximum over the North Atlantic in September–November (SON) corresponds well to that previously noted in Fig. 2. The region near 12°N and between 45° and 25°W only satisfies our low-OLR criteria in the months of October and November. NCEP wind reanalysis (Kalnay et al. 1996), overlain in Fig. 3, shows that the long-term mean wind direction

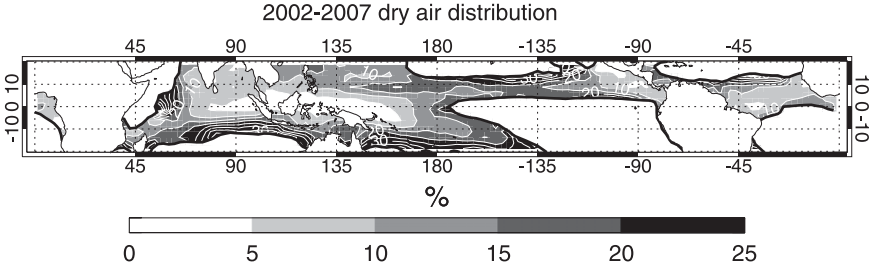

FIG. 2. Frequency of midlevel dry air layers over the tropical oceans within each 2.5° bin. Shading marks each frequency change between 0% and 25%, with white contours marking further changes of every 5% (if applicable). The thick black line marks the maximum extent of where the monthly mean OLR for at least one month in the calendar year is less than 240 W m^{-2}; only those grid areas for which this criterion is satisfied have frequency contours provided.

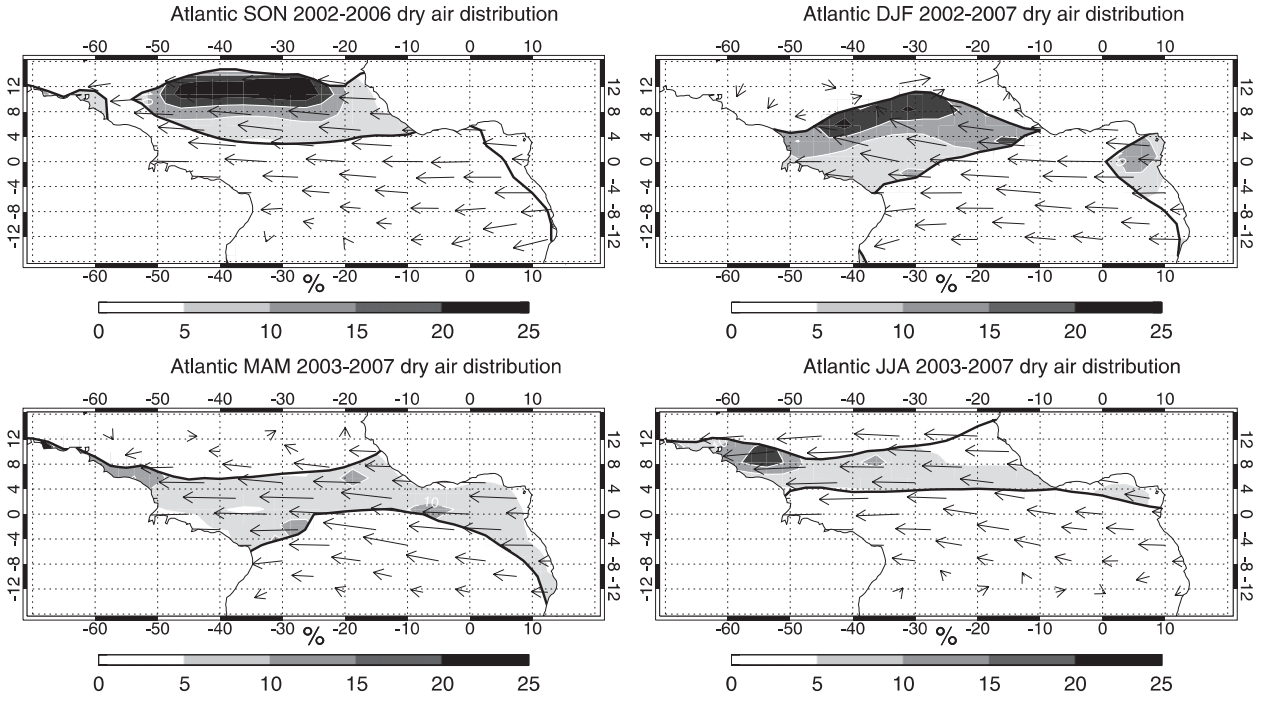

FIG. 3. As in Fig. 2, but over the Atlantic Ocean, separated by season, and with seasonal mean 500-hPa wind vectors overlain.

over this area at 500 hPa during SON is from the east-southeast, suggesting that wind flow at this height is climatologically from the African continent; the origins of these particular air parcels will be examined in further detail in section 4. High occurrence of dry air is also seen in December–February (DJF) closer to 8°N.

The frequency of dry air layers is much lower in March–May (MAM) and June–August (JJA). Mean 500-hPa winds during these months are from the east, similar to SON. In DJF, however, mean flow is more variable, with winds south of 8°N from the east and winds north of 8°N from the west.

The greater magnitude of dry air anomalies in SON also coincides with the farthest northward extent of our study area (i.e., long-term mean monthly OLR of <240 W m^{-2}). This would lead to a closer proximity of the study area to extratropical storm tracks in the subtropics (and even midlatitudes). It could then be postulated that the SON dry air anomalies are more likely to be related to extratropical influences than are those in the other seasons, even though this is not suggested by the mean direction of flow for these months. This theory will also be tested in section 4.

b. Indian Ocean

Figure 2 shows a maximum in dry air frequency of ~50% over the western Indian Ocean (i.e., near the equator and around 57°E). High values from 20% to 40% are also noted in the southeast (around 12°S and 70°–120°E). A large portion of the Indian Ocean (from 4°S to 20°N and 70° to 100°W) shows low occurrence of dry air observations.

Figure 4 shows the largest dry air maxima in JJA and SON, with smaller frequencies noted in DJF and MAM. June–November also happens to be when the Madden–Julian oscillation (MJO) signal is weaker (Madden and Julian 1994). This may be related to the warming and drying of the midtroposphere following the active phase of the MJO, as reported by Tian et al. (2006). In comparison with Fig. 2, it is clear that the western Indian Ocean peak is mostly due to layers in JJA (the active monsoon season), whereas the southeastern peak is strongest in SON. Though substantially lower in magnitude than those in June–November, minor peaks are noted in DJF near Sri Lanka and around 12°S, 80°E, as well as in MAM over 4°N, 60°E and off the coast of Madagascar. Note that these lower values are comparable to what constitutes a high concentration of dry air layers in the Atlantic (Fig. 3) because of the lower occurrence of dry air layers overall over the Atlantic versus the Indian Ocean.

c. Pacific Ocean

Figure 2 shows high dry air frequencies of ~30% over the central Pacific in the intertropical convergence zone (ITCZ) and close to 20°S in the South Pacific convergence

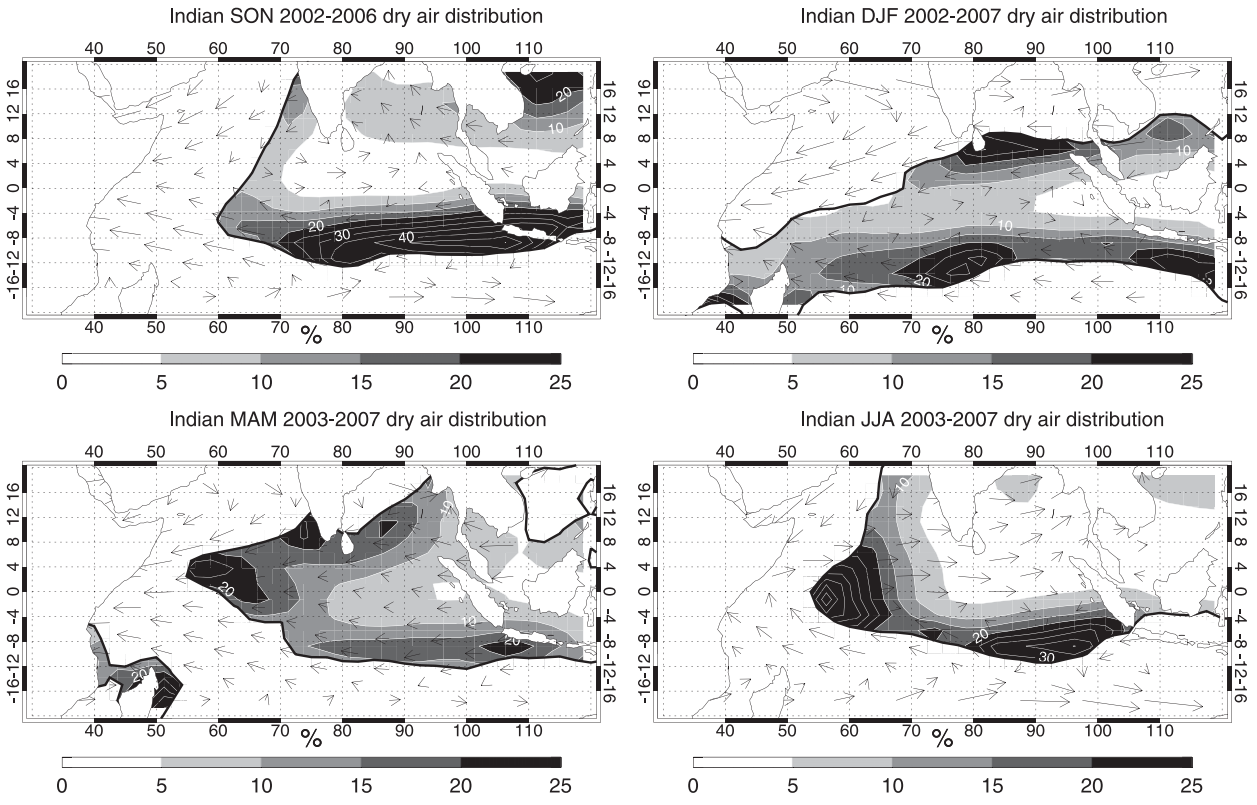

FIG. 4. As in Fig. 3, but over the Indian Ocean.

zone (SPCZ). Fewer dry air layers are observed close to the equator, where easterlies remain prevalent at 500 hPa year-round (Fig. 5). Closer to the subtropics, westerlies are seen more frequently depending on the extent of the tropical–subtropical boundary. The relation between westerlies and dry air layers will be discussed in the next section. Overall, dry air layers appear to be present at least 10% of the time basinwide, except in the far eastern Pacific and over the warm-pool region of the western Pacific.

Figure 5 shows that the highest frequency of dry air layers is in DJF, with smaller frequencies in the other seasons. Areas of maximum occurrence in SON are in the central Pacific, north of the Philippines, and along the eastern edge of the SPCZ. During the EPIC campaign (Zuidema et al. 2006), the R/V *Ronald Brown* was located at 10°N, 95°W during September; Fig. 5 shows that dry air layers occur in this region 5% of the time during SON. In DJF, maximum values are seen in a long swath near 10°N, 120°E–160°W, along the southern boundary near 20°S, 150°E–140°W, and in the eastern Pacific near 10°N, 120°W. The TOGA COARE field program observing period was from 1 November 1992 to 28 February 1993, over a region roughly bounded by 140°E, 180°, 10°S, and 10°N (Webster and Lukas 1992); Fig. 5 shows that the frequency of dry air layers varies greatly in this region, from 0% to 35% occurrence. Observations in MAM remained roughly in the same areas as in DJF, although the magnitudes were substantially decreased.

In JJA, only two weak maxima are noted, one near 10°S, 180° and another near 10°N, 150°W. The mean 500-hPa flow across 10°N latitude during JJA is largely from the east. However, over 150°W longitude, the winds have a slight southward component (i.e., from the subtropics) while the winds from areas to the east and west have a slight northward component. Meanwhile, winds south of the SPCZ maximum shift from eastward (near 20°S) to westward (near 10°S). This shift within a close proximity on a climatological scale suggests a greater opportunity for mixing of tropical and extratropical air in this location, suggesting that dry air layers over the area during austral winter may originate in the extratropics.

4. Locations of dehydration

Trajectories backward in time from observation to 20 days prior were calculated for each midlevel dry air region using a trajectory program that uses 3D NCEP

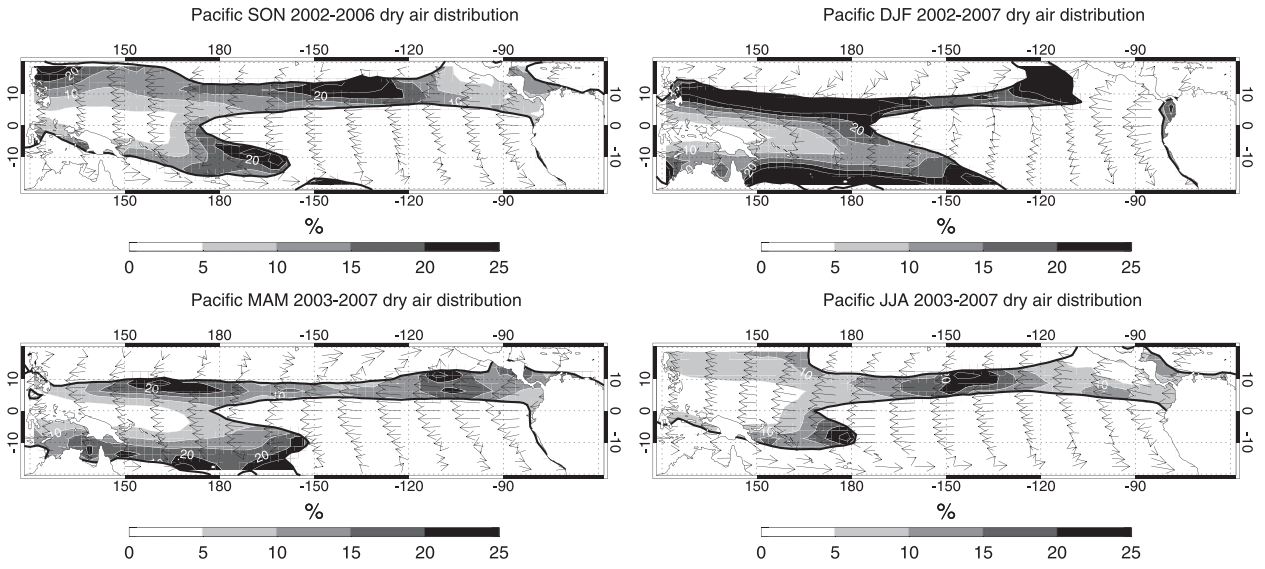

FIG. 5. As in Fig. 3, but over the Pacific Ocean.

winds as described in Bowman (1993). Trajectories were initialized at the location of each dry retrieval in AIRS, version 5, at 500 hPa in height and 0000 UTC. We calculate RH for each time step of the trajectory using the AIRS-measured value at the end of the trajectory and NCEP temperature interpolated to each time step (6 h back in time). Although AIRS also provides temperature measurements, the nature of back-trajectory analysis requires temperatures at specific points and times along the trajectory, something that AIRS is not able to provide given its orbit; therefore, the NCEP temperature is used. Our goal is to find the most recent time at which each trajectory was saturated (i.e., reached 100% RH). If we assume that this is the last time condensation occurred, then this point is the location at which the parcel's humidity was set. This is a well-validated approach to estimating tropical water vapor (see Dessler and Minschwaner 2007 and references therein). Although individual AIRS measurements, as mentioned before, are accurate to within ~10%, Dessler and Sherwood (2000), while using a similar model, noted that errors may also arise from physical processes not included in the model, errors in the NCEP wind and temperature fields, and/or unresolved motions in the wind fields. Dessler and Sherwood (2000), however, also noted that situations arising from these did not lead to serious systematic errors.

Figure 6 shows two sample back trajectories calculated from this method, using observations over the Atlantic Ocean in September of 2002. Stars at the end of the trajectory mark the location of observation by AIRS. Thick black lines mark where the long-term mean OLR for September is less than 240 W m^{-2}, and thin black lines mark the country outlines for geographical reference. This figure shows that, although the locations for observation are similar for the two, the source regions are very different. On the left, the back-trajectory path goes to the northeast, ending over Libya. On the right, the path goes to the southeast, with a location of dehydration identified over the southern Atlantic.

Figure 7 shows the relative frequency of time from saturation to observation, separated by season. The area under each curve integrates to 1. It appears that the mean time since saturation is 5 days, with an exponential drop-off into longer time periods. The trajectories were only processed out to 20 days for computational reasons, although it appears that for about 10% of the back trajectories the air parcels had not yet reached saturation by this time. It is clear that the time from saturation to observation is about 5–6 days from September through May, whereas the maximum time period from June to August is 7 days, with many more trajectories lasting for 10 days or more.

The greatest number of JJA dry air observations comes from the Indian Ocean, where, according to Fig. 4d, most are viewed southwest of Sumatra and southeast of Somalia. The 500-hPa JJA winds near Sumatra are typically light, which would allow dry air layers to remain dry in the absence of turbulent mixing, allowing them to be viewed multiple times by the *Aqua* satellite as they slowly drift westward. Winds typically increase near 80°W, shifting from a westward trajectory to northwestward and then to a northward trajectory. This path may bring these dry air layers directly into the second identified location of dry air noted off the Somali coast, thus sampling the same feature in additional overpasses.

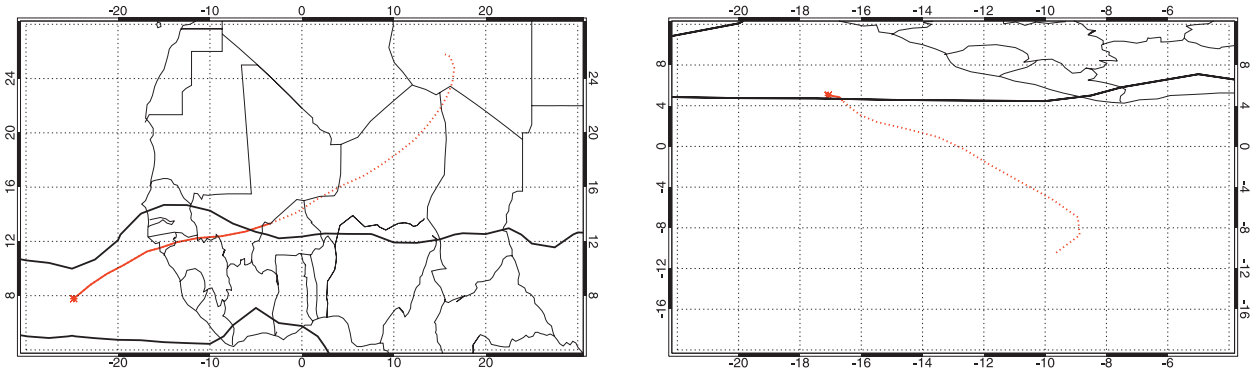

FIG. 6. Two sample calculated back trajectories (red lines) calculated from observations over the Atlantic Ocean in September 2002. Stars at the end of the trajectory mark the location of observation by AIRS. Thick black lines mark where the long-term mean OLR for September is less than 240 W m^{-2}, and thin black lines mark country outlines for geographical reference. The dashed part of the red line marks the trajectory path for which the long-term mean OLR for June is greater than 240 W m^{-2}.

Upon investigation of this (not shown), it was noted that 1/3 of Indian Ocean JJA back trajectories were sampled twice. Two such trajectories from June 2003 are shown for reference in Fig. 8. This combination of light wind conditions and the potential for multiple sampling is only seen in the Indian Ocean during JJA and is not seen in the other two ocean basins. This result suggests that the longer time between saturation and observation during JJA than in the other seasons can be traced back to Indian Ocean conditions during these 3 months.

To answer the question of whether these dry layers were last saturated over land or ocean, a simple land/ocean mask was checked at the location of dehydration identified through trajectory analysis. Table 1 lists the percentage of dry air observations that were last saturated over the ocean. This table shows that, in every ocean basin and every season, oceanic origins are more common than land origins. The Indian and Pacific Oceans have dry air layers originating from ocean regions 70.1% and 81.4% of the time, respectively. A higher percentage of oceanic sources for the Pacific Ocean would be expected, given the larger size of this basin. The Atlantic Ocean, by contrast, has both the lowest percentage of oceanic origins (69.1%) and the greatest spread between seasons, with nearly 40% of dry air parcels being last saturated over land during JJA.

a. Atlantic Ocean

The shading in Fig. 9 indicates the relative locations of dehydration for parcels originating over the Atlantic Ocean, separated into season and binned into 15° × 15° boxes. The total of all values in shading add up to unity. Mean trajectories are computed from the center of each 15° × 15° box that contributes at least 1% of the total observed midlevel dry air layers. These mean trajectories are plotted in red.

In boreal autumn and winter (Fig. 9, top panels), the shading indicates that most dry air layers originate in the northern Atlantic. In boreal spring and summer (Fig. 9, bottom panels), the southeastern Atlantic is a more prominent source region. The 500-hPa winds from March to August over this region have a more northward component than those from September to February, thus bringing air toward the equator rather than simply toward the west. In addition, layers originate from North Africa during all seasons. Galewsky et al. (2005) and Dessler and Minschwaner (2007) identified similar trajectories in the North Atlantic and North Africa to be parcels riding up the isentropes and cooling as they mix reversibly into midlatitudes. This tropical air then condenses and loses water; when it then returns to the tropical regions, the air is drier than it was when it left.

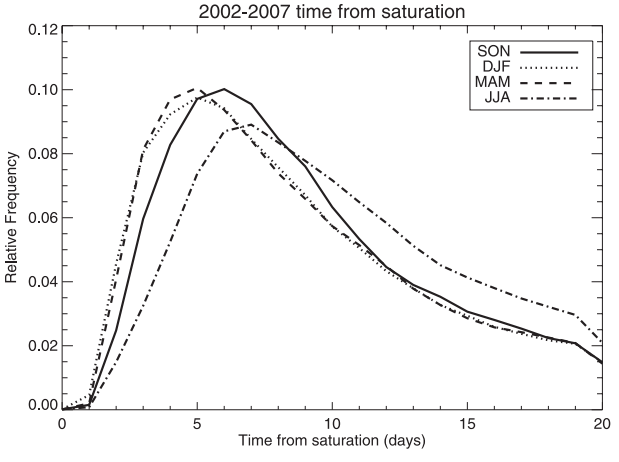

FIG. 7. Relative frequency distribution of the time between parcel saturation and observation, binned by day and separated by season. The sum under each curve adds to unity.

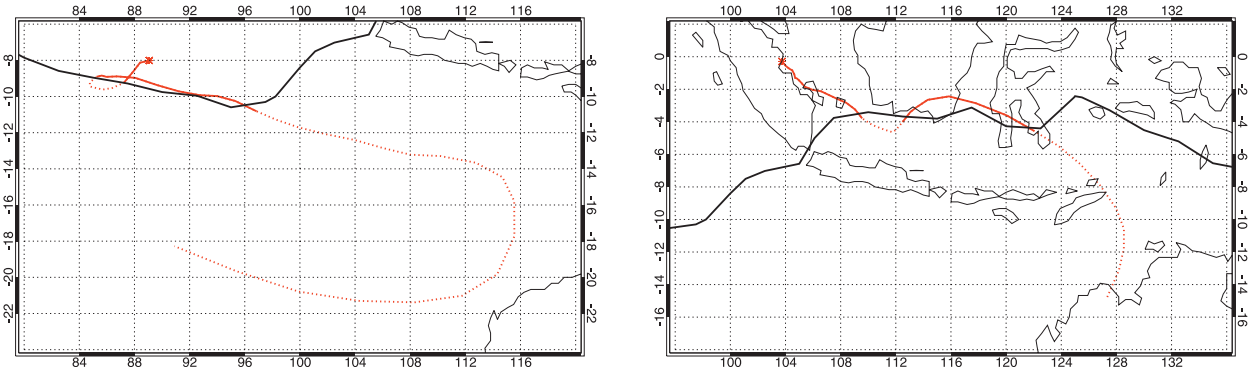

FIG. 8. As in Fig. 6, but for observations over the Indian Ocean in June 2003.

The mean trajectories that originate in the North Atlantic travel mostly southward in SON, move more southeastward in DJF and MAM, and travel little in JJA. In comparing Figs. 3 and 9, it is apparent that, with the exception of DJF, these parcel back trajectories from the North Atlantic do not coincide with time periods during which the climatological mean 500-hPa winds are from the north. This suggests that many of the studied back trajectories do not coincide with climatological mean winds, lending credence to the argument that these observations of very dry air are anomalous.

The mean trajectories that originate in the South Atlantic travel northwestward, with pronounced curves around 15°S where the climatological winds change from northwestward to northeastward. This shift from midlatitude westerlies to tropical easterlies is also evident in the trajectories originating in East Africa. In DJF and MAM, the East African mean trajectories appear to converge from their varied origins into a close grouping just north of the equator.

b. *Indian Ocean*

Figure 10 shows that, regardless of season, the majority of dry air layers entering the Indian Ocean come from the southern subtropical ocean. Trajectory analysis of the layers originating in the south Indian Ocean shows largely northeastward transport until about 15°S, when the winds shift to northwestward. The endpoints of the average trajectories for SON and JJA point toward the eastern and western Indian Ocean, respectively. Southeastward flow between Indonesia and Australia during JJA may ''block'' flow from the extratropics west of 90°E, whereas more northerly flow west of 90°E allows more extratropical air to travel into the tropics.

More variety is seen in the endpoints of the trajectories of the layers from the north. In SON layers generally move eastward into the South China Sea (included in this paper as part of the Indian Ocean because of geographic convenience). From December to May, Northern Hemisphere trajectories move southeastward into the Bay of Bengal (mostly in DJF) and peninsular India (mostly in MAM). Northern Indian Ocean dry air layers originate predominantly over the Arabian Sea. A majority of this region's dry air layers occur in boreal spring (mostly in May; not shown), just preceding the onset of the Indian monsoon. These high counts are followed by much lower counts in boreal summer, most likely resulting from the oceanic flow northward onto the Indian subcontinent during the monsoon months. The onset of the monsoon in June is very apparent, as seen in the low-count trajectories originating from the Middle East, curving southward before reaching peninsular India, and ending in the Arabian Sea.

c. *Pacific Ocean*

The shading in Figure 11 shows that there is a greater spread in the locations of dry air origin over the Pacific than in the previous two ocean basins. This, however, is mostly because the Pacific is a larger basin. The North and east Pacific predominate as source regions throughout the year. Dry air frequently originates in Australia, especially from December to May. Lower frequencies are seen from the southeast Pacific, southern and Southeast Asia, and the Caribbean Sea.

The first interesting feature of the mean trajectories is the grouping of mean trajectories from southern and Southeast Asia in each season except JJA. Parcels

TABLE 1. Percentage of dry air observations that originate over oceanic regions.

	Atlantic	Indian	Pacific
SON	80.8%	69.1%	83.7%
DJF	69.8%	73.9%	77.4%
MAM	63.9%	66.6%	75.7%
JJA	61.8%	70.8%	88.6%

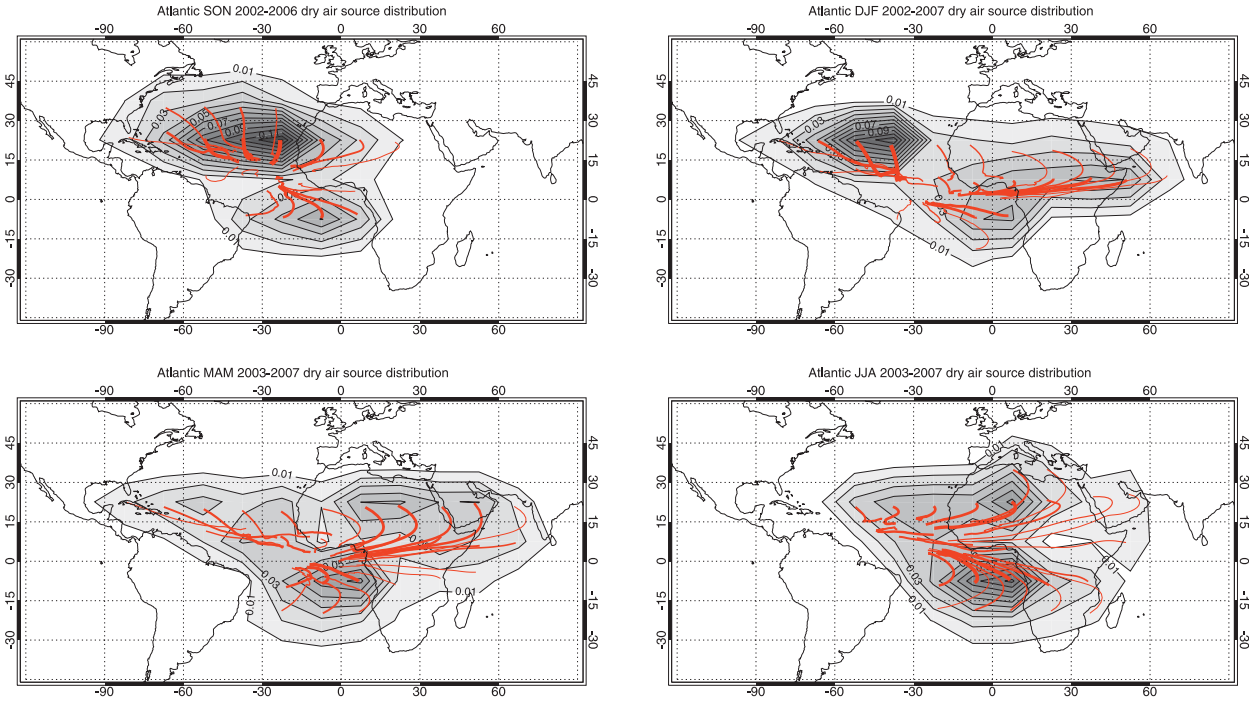

FIG. 9. Relative frequency of dry air layer source regions for the Atlantic Ocean, grouped into 15° bins and separated by season. The sum of all contoured values adds to unity. Red lines mark the mean trajectory from each bin where the relative frequency is greater than 1%. The thickness of each red line is proportional to the relative frequency from the associated bin.

along these trajectories travel along the subtropical jet around 20°N until around 150°E, where 500-hPa flow is climatologically southward these times of the year. Upon encountering this flow, the parcels curve southeastward and settle into the northwest Pacific. Redelsperger et al. (2002), as mentioned in the introduction, analyzed dry air layers observed during TOGA COARE. By looking at Fig. 11 and focusing on this region (°°10°S–10°N, 140°W–180°) during DJF, it can be seen that mean trajectories enter this region predominantly from the north. While more tropical convection was noted during TOGA COARE in the southern half of the study area, no mean trajectories enter this region from the southern half. Thus, Fig. 11 suggests that the dry air layers analyzed during TOGA COARE may have originated in southern and/or Southeast Asia before entering the study area from the north.

Trajectories from the North Pacific appear to slowly move southward, with some of the trajectories showing clear southwestward curves. The curve is more prominent in trajectories from the Caribbean Sea, with the trajectories ending along a westward track as the parcels settle in the east Pacific. Zuidema et al. (2006) calculated two back trajectories (20 and 22 September 2001) initialized at 10°N, 95°W, where the R/V *Ronald H. Brown* was located during the EPIC campaign. The trajectory for 20 September tracked east-northeast toward Central America; this would seem to agree with a mean trajectory traveling from the Caribbean, as seen in SON according to Fig. 11. The 22 September trajectory tracked south toward the equator; not precisely in line with our calculated mean back trajectories but close enough so that this 22 September case should not be seen as anomalous.

Trajectories originating over Australia move north and northeastward into the SPCZ. Many endpoints of the mean trajectories from the southeast Pacific appear to end in the central Pacific, in an area not included in the dry air distribution analysis (cf. to the boldface OLR outline in Fig. 6). Parcels originating from these southeast Pacific regions appear to disperse evenly between toward the ITCZ and toward the SPCZ, leaving a mean trajectory pointing to the area between.

5. Conclusions

Whereas previous studies have noted midlevel dry air layers over specific regions in the Pacific Ocean based on case studies, this paper looks at all warm oceanic areas using the criterion that, for at least one month, the monthly mean OLR over that area is less than 240 W m^{-2}. We use a definition of dry air layers of RH <20%. Let us now revisit the questions raised in the introduction:

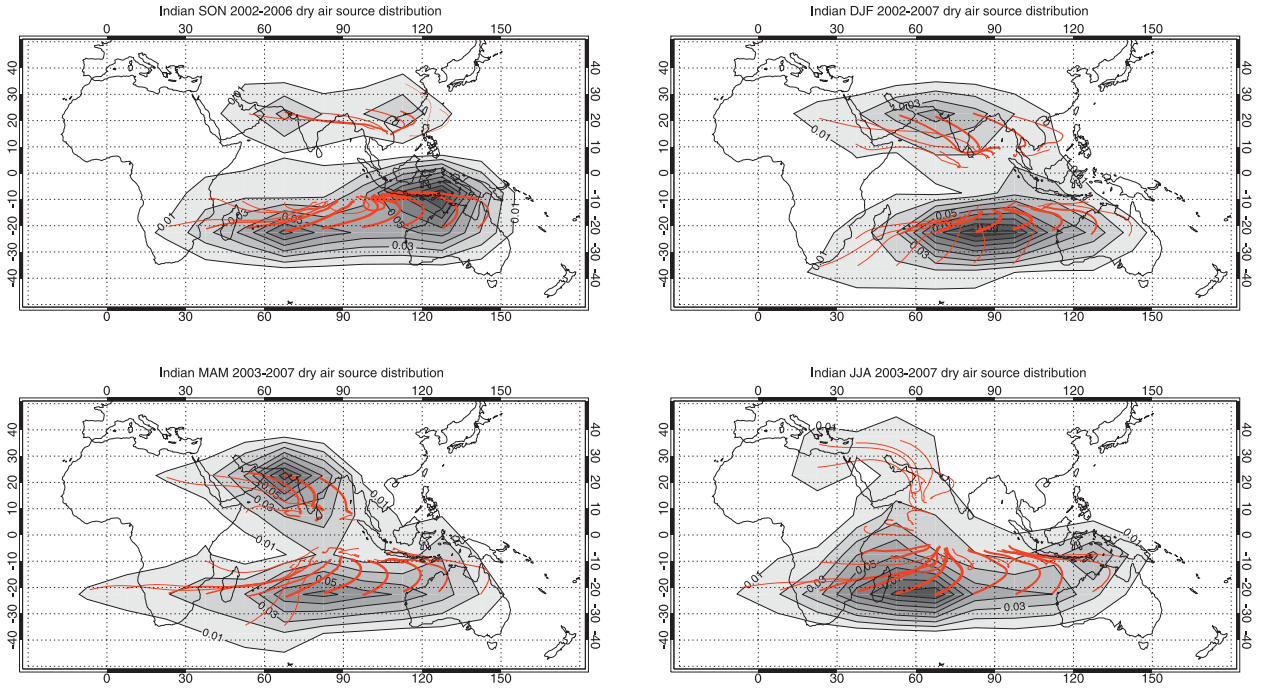

FIG. 10. As in Fig. 9, but for the Indian Ocean.

What is the applicability of the previous Pacific Ocean regional case studies to the rest of the basin? Large variations in the spatial and seasonal distribution of midlevel dry air layers exist across the Pacific. This high degree of variation suggests limits on the applicability of case-study trends and observations of dry air layers to the Pacific as a whole. Although field campaigns such as TOGA COARE and EPIC have contributed greatly to our understanding of tropical meteorology, studies may be needed in other regions to describe more accurately the regional nature and effects of midlevel dry air layers.

Can these be applied to the Indian and Atlantic Oceans as well, or are there clear differences among the three basins? When compared with the Pacific Ocean, the Indian Ocean has a similar dry air CDF, and both basins see relatively fewer dry air layers in MAM when

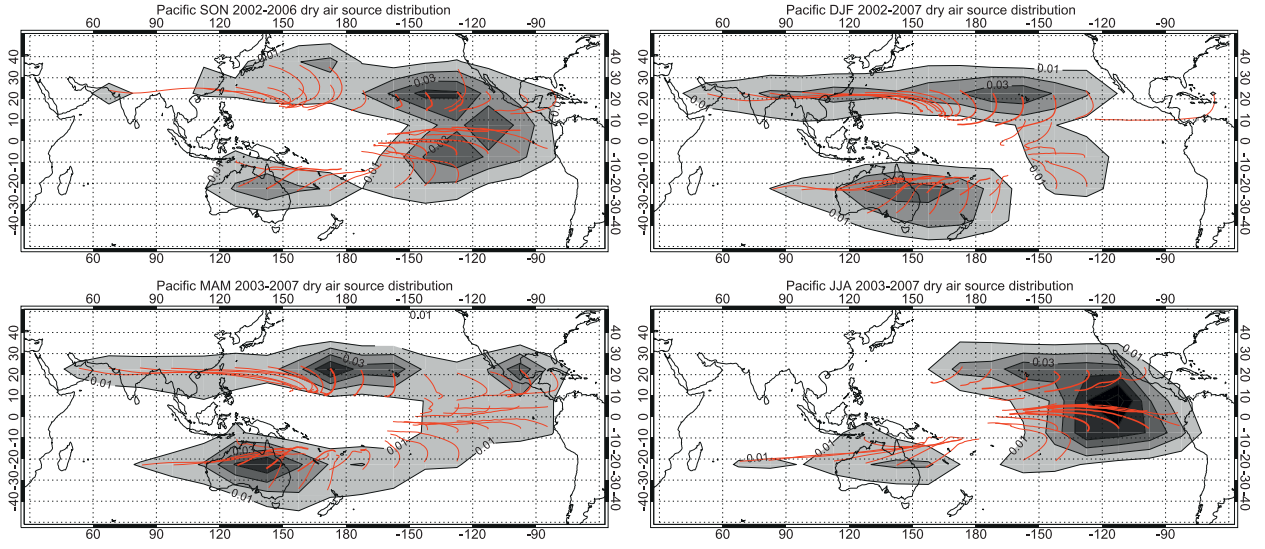

FIG. 11. As in Fig. 9, but for the Pacific Ocean.

extratropical-to-tropical winds are seen climatologically only in localized areas such as the Indian subcontinent, Australia, and near 10°N, 160°E. However, the spatial distribution of layers appears to be more localized in the Indian Ocean, with maxima approaching 50% occurrence in SON and JJA (when winds are generally lighter) as compared with the Pacific where layers are rarely seen more than 30% of the time and winds are stronger year-round. The Atlantic Ocean sees fewer dry air layers than the Indian and Pacific Oceans, not simply because of the smaller extent of warm tropical ocean, but also in terms of relative distribution. Table 1 shows that the Atlantic Ocean receives more dry air parcels from continental sources; thus, one would expect to see as many or more dry air layers overall as in the other two basins, because continental air is usually drier than maritime air. This discrepancy lends credence to concerns that the AIRS instrument may give artificially high values of relative humidity in the presence of high aerosol optical depths, as would be seen in dusty air from over the Sahara (S. Wong 2008, personal communication).

How does the distribution of such layers vary by season? The seasonal distribution of midlevel dry air layers shows a wide amount of variation. In the Atlantic, most layers occur in SON, with the least in MAM. The locations of maxima appear to be limited to the northern Atlantic. More variation is present in the locations of maxima in the Indian Ocean, moving from the west in JJA (the active monsoon season) to the southeast in SON, with fewer layers observed in DJF and MAM. The Pacific Ocean sees many more layers in DJF, with a sharp drop-off into MAM. The spatial distribution of layers in the Pacific also varies, though the variation is less than that in the Indian Ocean since the Pacific experiences wind changes (in magnitude and direction) of a smaller scale than are seen in the Indian Ocean.

Where do these dry air layers originate, and how does this distribution vary seasonally? Back trajectories for all three regions suggest that most midlevel dry air layers come from the subtropics, though some variability exists. There appears to be a seasonal pattern in dry air layers, with more seen from the north in DJF and from the south in JJA (i.e., each hemisphere's respective winter). This should be expected as the jet streams move poleward in the winter hemisphere, allowing more mixing from the midlatitudes into the tropics; an example of this was noted in Fig. 11 over the TOGA COARE region. All ocean basins see trajectories from both oceanic and continental sources, although more dry air layers originate over the ocean. Some regions are the origins for different oceans depending on season (or, in the case of the Arabian Sea, provide midlevel dry air layers to all three oceans). The Atlantic and Pacific Oceans both have what appear to be jet streams from continental regions (Africa for the Atlantic, Southeast Asia for the Pacific) acting as sources of dry air.

Many questions remain with regard to midlevel dry air layers. How does the source region (i.e., oceanic vs continental) affect the layer's thickness, area, and so on? Does variation exist with respect to longer-term climatological issues, such as the El Niño–Southern Oscillation? Also, the initial question of relating dry air layers and cumulus congestus clouds on a global scale remains.

Acknowledgments. Many thanks are given to Sun Wong, Kenneth Bowman, Paquita Zuidema, and Eric Fetzer for their advice and guidance. This work was supported by the NASA Earth System Science Fellowship. AIRS data were obtained from the Goddard Space Flight Center's Data and Information Services Center (DISC). NCEP reanalysis-derived data were provided by the NOAA/OAR/ESRL PSD of Boulder, Colorado, from their Web site (http://www.cdc.noaa.gov/).

REFERENCES

Bowman, K. P., 1993: Large-scale isentropic mixing properties of the Antarctic polar vortex from analyzed winds. *J. Geophys. Res.,* **98,** 23 013–23 027.

Brown, R. G., and C. Zhang, 1997: Variability of midtropospheric moisture and its effect on cloud-top height distribution during TOGA COARE. *J. Atmos. Sci.,* **54,** 2760–2774.

Ciesielski, P. E., R. H. Johnson, P. T. Haertel, and J. Wang, 2003: Corrected TOGA COARE sounding humidity data: Impact on diagnosed properties of convection and climate over the warm pool. *J. Climate,* **16,** 2370–2384.

Dessler, A. E., and S. C. Sherwood, 2000: Simulations of tropical upper tropospheric humidity. *J. Geophys. Res.,* **105,** 20 155–20 163.

——, and K. Minschwaner, 2007: An analysis of the regulation of tropical tropospheric water vapor. *J. Geophys. Res.,* **112,** D10120, doi:10.1029/2006JD007683.

Fetzer, E. J., Ed., 2005: Validation of AIRS/AMSU/HSB core products, for data release version 4.0. JPL Rep. D-31448, 60 pp.

Galewsky, J., A. Sobel, and I. Held, 2005: Diagnosis of subtropical humidity dynamics using tracers of last saturation. *J. Atmos. Sci.,* **62,** 3353–3367.

Jensen, M. P., and A. D. Del Genio, 2006: Factors limiting convective cloud-top height at the ARM Nauru Island climate research facility. *J. Climate,* **19,** 2105–2117.

Johnson, R. H., P. E. Ciesielski, and K. A. Hart, 1996: Tropical inversions near the 0°C level. *J. Atmos. Sci.,* **53,** 1838–1855.

——, T. Rickenbach, S. A. Rutledge, P. Ciesielski, and W. Schubert, 1999: Trimodal characteristics of tropical convection. *J. Climate,* **12,** 2397–2418.

Kalnay, E., and Coauthors, 1996: The NCEP/NCAR 40-Year Reanalysis Project. *Bull. Amer. Meteor. Soc.,* **77,** 437–471.

Liebmann, B., and C. A. Smith, 1996: Description of a complete (interpolated) outgoing longwave radiation data set. *Bull. Amer. Meteor. Soc.,* **77,** 1275–1277.

Madden, R. A., and P. R. Julian, 1994: Observations of the 40–50-day tropical oscillation—A review. *Mon. Wea. Rev.,* **122,** 814–837.

Parsons, D. B., K. Yoneyama, and J. L. Redelsperger, 2000: The evolution of the tropical western Pacific atmosphere-ocean system following the arrival of a dry intrusion. *Quart. J. Roy. Meteor. Soc.,* **126,** 517–548.

Pierrehumbert, R. T., 1995: Thermostats, radiator fins, and the local runaway greenhouse. *J. Atmos. Sci.,* **52,** 1784–1806.

Redelsperger, J.-L., D. Parsons, and F. Guichard, 2002: Recovery processes and factors limiting cloud-top height following the arrival of a dry intrusion observed during TOGA COARE. *J. Atmos. Sci.,* **59,** 2438–2457.

Ryoo, J. M., D. W. Waugh, and A. Gettleman, 2008: Variability of subtropical upper tropospheric humidity. *Atmos. Chem. Phys.,* **8,** 2643–2655.

Simpson, J., 1992: Global circulation and tropical cloud activity. *The Global Role of Tropical Rainfall,* J. S. Theon et al., Eds., A. Deepak Publishing, 77–92.

Spencer, R. W., and W. D. Braswell, 1997: How dry is the tropical free troposphere? Implications for global warming theory *Bull. Amer. Meteor. Soc.,* **78,** 1097–1106.

Tian, B., D. E. Waliser, E. J. Fetzer, B. H. Lambrigtsen, Y. L. Yung, and B. Wang, 2006: Vertical moist thermodynamic structure and spatial–temporal evolution of the MJO in AIRS observations. *J. Atmos. Sci.,* **63,** 2462–2485.

Waugh, D. W., and L. M. Polvani, 2000: Climatology of intrusions into the tropical upper troposphere. *Geophys. Res. Lett.,* **27,** 3857–3860.

——, and B. M. Funatsu, 2003: Intrusions into the tropical upper troposphere: Three-dimensional structure and accompanying ozone and OLR distributions. *J. Atmos. Sci.,* **60,** 637–653.

Webster, P. J., and R. Lukas, 1992: TOGA COARE: The Coupled Ocean–Atmosphere Response Experiment. *Bull. Amer. Meteor. Soc.,* **73,** 1377–1416.

Yoneyama, K., and D. B. Parsons, 1999: A proposed mechanism for the intrusion of dry air into the tropical western Pacific region. *J. Atmos. Sci.,* **56,** 1524–1546.

Zachariasse, M., H. G. J. Smit, P. F. J. van Velthoven, and H. Kelder, 2001: Cross-tropopause and interhemispheric transports into the tropical free troposphere over the Indian Ocean. *J. Geophys. Res.,* **106,** 28 441–28 452.

Zhang, C., B. E. Mapes, and B. J. Soden, 2003: Bimodality in tropical water vapour. *Quart. J. Roy. Meteor. Soc.,* **129,** 2847–2866.

Zuidema, P., B. Mapes, J. Lin, C. Fairall, and G. Wick, 2006: The interaction of clouds and dry air in the eastern tropical Pacific. *J. Climate,* **19,** 4531–4544.